

Metal–nanocarbon contacts

This content has been downloaded from IOPscience. Please scroll down to see the full text.

2014 Semicond. Sci. Technol. 29 054006

(<http://iopscience.iop.org/0268-1242/29/5/054006>)

View [the table of contents for this issue](#), or go to the [journal homepage](#) for more

Download details:

IP Address: 129.210.17.128

This content was downloaded on 02/04/2014 at 08:51

Please note that [terms and conditions apply](#).

Metal–nanocarbon contacts

Patrick Wilhite¹, Anshul A Vyas¹, Jason Tan¹, Jasper Tan¹,
Toshishige Yamada^{1,3}, Phillip Wang², Jeongwon Park² and Cary Y Yang¹

¹ Center for Nanostructures, Santa Clara University, Santa Clara, CA, USA

² Applied Materials Inc., Santa Clara, CA, USA

³ Electrical Engineering, University of California, Santa Cruz, CA, USA

E-mail: patrick.wilhite@gmail.com

Received 13 November 2013, revised 28 December 2013

Accepted for publication 13 January 2014

Published 1 April 2014

Abstract

To realize nanocarbons in general and carbon nanotube (CNT) in particular as on-chip interconnect materials, the contact resistance stemming from the metal–CNT interface must be well understood and minimized. Understanding the complex mechanisms at the interface can lead to effective contact resistance reduction. In this study, we compile existing published results and understanding for two metal–CNT contact geometries, sidewall or side contact and end contact, and address key performance characteristics which lead to low contact resistance. Side contacts typically result in contact resistances $> 1 \text{ k}\Omega$, whereas end contacts, such as that for as-grown vertically aligned CNTs on a metal underlayer, can be substantially lower. The lower contact resistance for the latter is due largely to strong bonding between edge carbon atoms with atoms on the metal surface, while carrier transport across a side-contacted interface via tunneling is generally associated with high contact resistance. Analyses of high-resolution images of interface nanostructures for various metal–CNT structures, along with their measured electrical characteristics, provide the necessary knowledge for continuous improvements of techniques to reduce contact resistance. Such contact engineering approach is described for both side and end-contacted structures.

Keywords: nanotube, contact, resistance, interface, metal

(Some figures may appear in colour only in the online journal)

1. Introduction

Carbon-based nanostructures (or nanocarbons) such as carbon nanotubes (CNTs) [1–6], carbon nanofibers (CNFs) [7–9], and graphene [10–13] are candidate materials for next-generation semiconductor devices and integrated circuits (IC) due to their tolerance to electromigration under high currents and excellent electrical, thermal, and mechanical properties [14–24]. Nanocarbons show increasing promise to replace copper (Cu) for on-chip interconnects and through-silicon-vias in three-dimensional chips [25–26], largely because of their excellent controllability for directional growth and high current capacity. The key performance-limiting factor for metallic single-wall carbon nanotubes (m-SWCNTs), multi-wall carbon nanotubes (MWCNT, generally metallic), and CNFs remains the high contact resistance originating from the interface with metal electrodes [27]. While not unique to nanocarbons, the effect of contact resistance is enhanced as devices shrink [28], and is particularly problematic in the nanoscale [29].

In this paper, we review recent studies on metal–nanocarbon contacts in what is commonly known as local interconnects. Unlike global interconnects, the lengths of local interconnects, fabricated as part of the front-end IC technology, generally scale with on-chip dimensions. And the local and global interconnects together constitute the critical limiting factor in chip performance. Process considerations regarding integration of nanocarbons as interconnect materials have been addressed in the latest ITRS Roadmap [24] and by others [14, 16]. Despite their high quantum resistance, CNT and graphene are considered potential local interconnects in the first metal layer, where SWCNTs, double-wall CNTs, and graphene nanoribbons (GNRs) could perform on par or better than Cu, while MWCNTs show comparable performance for lengths larger than $0.5 \mu\text{m}$ [16, 24]. For global interconnects, virtually any nanocarbon has the potential to outperform Cu [14, 16, 24]. In 3D integration schemes, vertically aligned CNTs and horizontal graphene layers may be combined for interconnect architectures made solely from nanocarbons [30, 31], and hybrid Cu/CNT

systems have also been proposed [32]. While our present study focuses on the electrical transport across the metal–nanocarbon interface and its consequences on contact resistance in local interconnects, the same understanding is expected to be applicable to global interconnects as well. In most cases discussed here, the extracted contact resistance for nanocarbon test devices tends to be the dominant component of the measured total resistance. Contact resistance between graphene and metal has also proven to be problematic for realizing high-performance FET devices, diminishing the benefits of graphene’s high carrier mobility and posing a severe bottleneck for device functionalization [33–35]. Despite challenges in optimizing metal–nanocarbon contact resistance and realizing that nanocarbons possess the highest current capacities among all known materials, we believe that suitable contact engineering based on clear understanding of the metal–nanocarbon interface will eventually lead to device resistances acceptable to specific applications. Thus, understanding the physical origin of metal–nanocarbon contact resistance and reducing it as much as needed are essential for functionalizing these materials in applications where high electrical conduction is critical.

In most cases, as in other heterostructures, high contact resistance between metal and nanocarbon originates from carrier tunneling across the interface due to work-function difference between the two materials [36, 37]. It can also result from defects (including impurities) at and/or near the interface [36, 38] which introduce physical and chemical changes in either or both contacting materials. The tunneling mechanism is similar to that for a Schottky barrier between metal and semiconductor, such as in semiconducting SWCNT [39]. Although the resistivity of the nanocarbon itself is also an important factor for a given application, achieving the optimum resistivity value does not necessarily yield the desirable device performance unless the contact resistance is properly controlled and minimized.

Theoretically, when ideal contacts are made, the resistance at the interface is governed by the quantum limit of $R_0 = h/2e^2$ per conduction channel, assuming transparent contacts. This limit is material-independent and is based on the assumption of quantum point contacts. Accounting for two conduction channels per CNT shell, this resistance becomes $R_0/2 = 6.45 \text{ k}\Omega$. However, this ideal coupling between the two conduction channels of a graphene cylinder (i.e., SWCNT) to the electrode surface may not always be possible due to Coulomb blockade [40] or other suppression mechanisms [41]. Nevertheless, *ab initio* calculations predicted contact resistivities $\geq 24.2 \text{ k}\Omega \text{ nm}^2$ for a side-contacted single graphene layer with various metals, with Ti yielding the lowest value [42]. This result suggests that a nanoscale metal–CNT contact area such as $20 \text{ nm} \times 20 \text{ nm}$ could yield total device resistance dominated by the intrinsic CNT properties rather than contact resistance. More recently, high-quality contacts to graphene with palladium have been reported, together with an elaborate transport model that determines contact resistance [43]. Carrier transport through the interface is not only dependent on the coupling strength between graphene and metal, but also depends on the number of conduction modes

in the graphene under the metal [43]. Others have suggested that there are no inherent physical limitations for metal–CNT interfaces to be roadblocks in functionalizing CNT devices [14].

CNFs, despite their many CNT-like features and electrical characteristics, are often overlooked for potential interconnect applications where CNTs are considered a leading candidate to replace copper. Moreover, the differences between CNTs and CNFs are not always easy to discern even from high-resolution imaging, and the distinction appears infrequently in the literature [8, 9, 19]. In the next two sections, where the interface nanostructures are discussed in conjunction with contact geometries, the differences and similarities in nanostructure and electrical behavior between CNT and CNF will become apparent. Due to this inconsequential and unnecessary distinction, CNF will be grouped together with CNT in the ensuing narrative, unless the discussion specifically calls for such distinction.

Test devices consisting of a CNT bridging an electrode pair generally show very high as-fabricated resistance, typically in the range of a few tens of $\text{k}\Omega$ or more, and nonlinear current–voltage (I – V) characteristics, due largely to the formation of tunneling barriers as well as interfacial defects [37]. Such non-ohmic behavior has also been observed for vertical CNT via interconnects test structures [9, 44–46]. Generally, contact resistance can be improved by current stressing and/or metallization of the CNT contacts. In particular, current stressing results in linear I – V behavior and reduction in contact resistance down to a few $\text{k}\Omega$ or less. However, such improvements are not sufficient for contact resistance reduction and process reproducibility. Metallization techniques such as electron-beam-induced deposition (EBID) or ion-beam-induced deposition (IBID) provide significant performance enhancement for CNT devices resulting from improved metal–nanocarbon interfaces, and increase in the contact area between CNT and electrodes. Nevertheless, obtaining low-resistance side-contacted CNT devices still remains a daunting challenge. While EBID and IBID techniques have been used by the scientific community for some time, Bachtold *et al* [47] recognized that amorphous carbon deposition at the contacts yielded a drastic reduction in CNT contact resistance. This simple technique consists of illuminating the electron beam in a scanning electron microscope (SEM) over the contact area to allow the growth of a carbon film from the impurities in the SEM chamber [47]. EBID and IBID techniques have been used extensively to investigate metal–CNT contacts in studies of CNT interconnects [19, 47–50].

For interconnect via applications, high-density CNT growth is used to increase the number of conduction channels within the via cavity, which in turn yields a lower total via resistance. The as-grown metal–nanocarbon interface in vertically aligned CNTs (end contact) is expected to result in a relatively low contact resistance compared with that formed at the deposited metal electrode on the CNT sidewall (side contact). This difference in contact geometry leads to contrasting carrier transport across metal–CNT interfaces, as unsaturated carbon bonds at the base of the CNT can

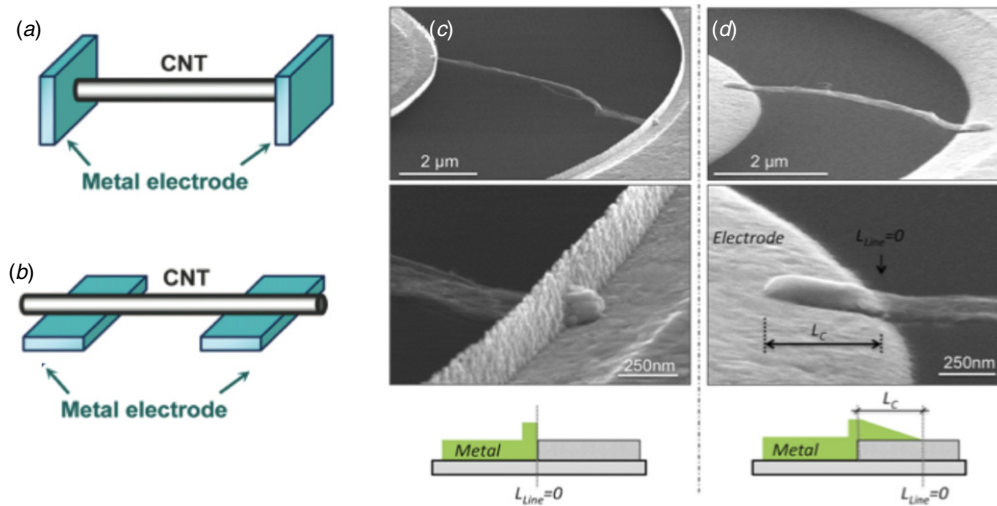


Figure 1. Schematic representation of two different metal-CNT contact configurations, (a) end contact and (b) side contact. An end-contact configuration exists for vertically grown CNTs. Reprinted with permission from the authors of [91]. Copyright 2010 American Chemical Society. SEM micrographs of CNT bundles suspended between two electrodes with (c) end contacts, and (d) a hybrid wrap-around configuration (side and end contacts). Reprinted with permission from the authors of [51]. Copyright 2013, AIP Publishing LLC.

easily latch onto the metal surface atoms, resulting in lower contact resistance for end-contacted structures [42, 51, 52]. This difference is illustrated in figure 1. However, unlike the horizontal side-contacted configuration, for a vertically grown end-contacted CNT, it is more challenging to separate the CNT and contact resistances from the measured total resistance due to difficulties in performing four-point probing (4PP). Nevertheless, contact resistance was successfully extracted for vertically aligned CNTs with various lengths and similar diameters [44, 53]. Another important consideration for a via structure lies in the control of the deposited top metal electrode, where the metal-nanocarbon interface is expected to behave differently from the as-grown interface. Reliable low-resistance patterned vias with each containing densely packed CNTs have proven to be an additional challenge in device functionalization [54].

In the following sections, research on side-contacted and end-contacted metal-CNT interfaces is reviewed. The emphasis of this paper is on the fundamental understanding obtained from experimental and modeling studies on the structure/electrical property relationships that lead to contact engineering techniques to reduce the metal-CNT contact resistance.

2. Side-contacted structures

A typical side-contacted structure is a CNT horizontally bridging two metal electrodes, shown schematically in figure 1(b), which is the focus of this section. One of the simplest and widely used fabrication methods consists of suspending a purified mixture of CNTs in an alcohol solution, which is then sonicated to de-bundle the CNTs, and then drop-casted on pre-patterned electrodes. Typical as-fabricated resistance values range from 10^4 to $10^9 \Omega$. Our experiments show that the initial I - V behavior tends to be highly nonlinear and asymmetric, and these effects are accentuated for devices with higher resistance. These initial resistances drop to the

$k\Omega$ range after stressing with a current of 10^5 - 10^6 A cm^{-2} . Since no appreciable degradations are observed in the CNT nanostructure using high-resolution electron microscopy, this drastic reduction in the total resistance is attributed to decrease in the contact resistance induced by localized Joule heating at the interface [14, 55]. A single-junction semi-empirical tunneling model supports this explanation, where an interfacial gap between CNF (also applicable to CNT) and metal, Au in this case, is reduced by current stressing [37]. When the gap separation shrinks, the I - V behavior becomes linear as the device resistance decreases and approaches ohmic, as illustrated in figure 2. While serving as a convenient modeling parameter, the existence of an interfacial gap is likely due to contact asperities and/or defects such as trapped adsorbates or residual impurities from device fabrication. The transport across the gap is similar to that through a Schottky barrier at a metal-semiconducting SWCNT contact [39]. Whereas for metal-semiconductor contact, tunneling is the direct result of inherent materials properties, namely, work-function difference, tunneling across the metal-CNT interface is most likely due to a combination of factors as stated above.

The considerations leading to modeling with an interfacial gap between a side-contacted graphene sheet and metals were formulated using density functional theory (DFT) and Green's function method [42]. In order to calculate contact resistances, the interaction energy for such metal-graphene contact was computed for various metals to determine the separation between adjacent layers, as shown in figure 3. From these calculations, Ti exhibits the strongest bonding with graphene with a separation slightly above 2.1 \AA , compared with the interplanar spacing of $\sim 3.5 \text{ \AA}$ for graphite. The suitability of the metals was assessed in ascending order of contact resistance, Ti, Pd, Pt, Cu, and Au, with Ti yielding the smallest separation leading to the smallest contact resistance. Additional modeling for a metallic SWCNT (7,7) resulted in a contact resistance of just $6.9 \text{ k}\Omega \text{ nm}^{-1}$ with Ti, due in part to a much smaller separation induced by the sidewall

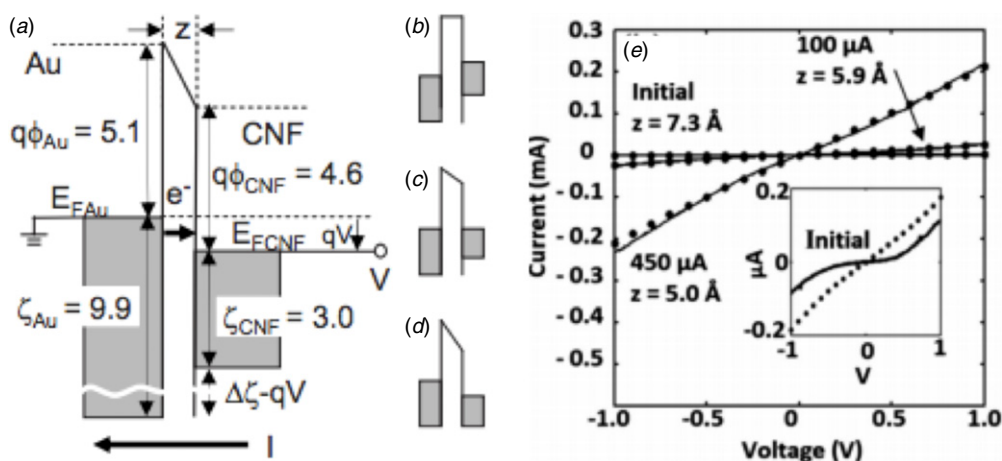


Figure 2. (a) An energy-band model for Au-CNF (assuming CNT band parameters) contact with a tunneling gap of spacing z and voltage V between them, $q\phi$ is work function, ζ is Fermi energy measured from the bottom of the Au valence band, and E_F is Fermi level position. $\Delta\zeta = \zeta_{FAu} - \zeta_{FCNF}$ is the difference between Au and CNF Fermi energies. The energy-band diagram is shown for (b) $V = 0$, (c) $V = 0$, and (d) $V > 0$. (e) Measured $I-V$ before and after multiple current stressing cycles, with current-stressing conditions shown. Solid circles are modeling results at 300 K, fitted to measured $I-V$ data, resulting in $z = 7.3, 5.9,$ and 5.0 Å. The inset shows improvement in $I-V$ linearity upon current stressing, with solid line indicating initial behavior. Reprinted with permission from the authors of [37]. Copyright 2010, AIP Publishing LLC.

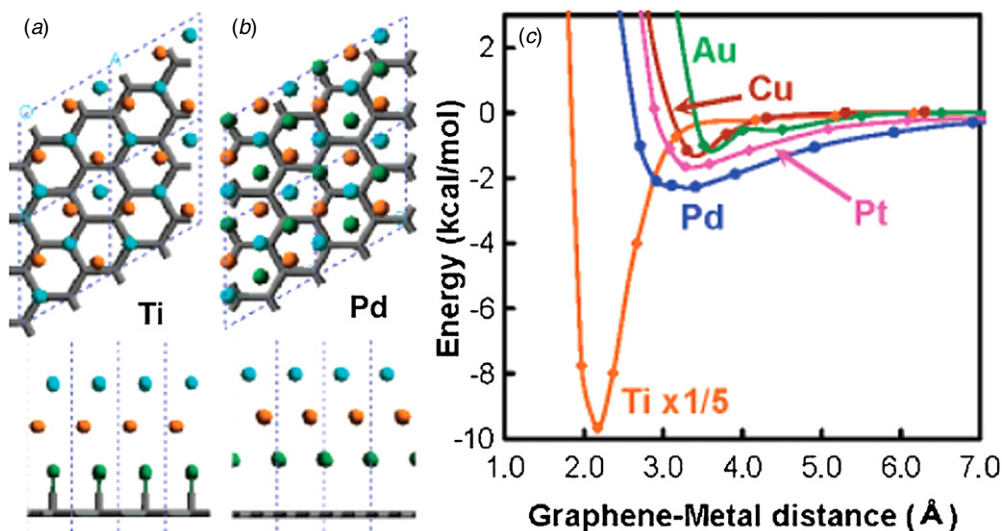


Figure 3. DFT-optimized positions for a graphene surface on (a) Ti and (b) Pd. (c) Interaction energy versus electrode separation between a graphene sheet and various metals. Ti shows the strongest binding which can lead to low contact resistance. Reprinted with permission from [42]. Copyright 2007, American Chemical Society.

curvature. These computed contact resistances are remarkably low compared to others reported in the literature. For example, using the semi-empirical tunneling model [37] for Au-CNT interface with a contact area of $0.125 \mu m^2$ (from SEM) and fitting the computed results to experimental $I-V$ curves yielded an interfacial gap of 5 Å and an estimated contact resistance of ~ 10 k Ω . Using the DFT model [42] for the same contact area would yield an Au-graphene contact resistance of just a few hundred ohms, for a gap of 3.5 Å. In comparing these results, one must keep in mind that the DFT model assumes monocrystalline structures in deducing the optimum gap separation, whereas in the semi-empirical model, the gap separation is a parameter used to fit the measured data. Regardless of the true physics of this interfacial gap, it is nonetheless a useful parameter for contact metal selection in side-contacted CNT structures.

Another important consideration for side-contacted CNTs is its ambient reactivity. Considering a monocrystalline sp^2 graphitic structure with no dangling bonds, CNTs are highly susceptible to their environment due to the non-localized π -electrons which results in van der Waals bonding out of the graphene plane [56–59]. This weak bonding from electrostatic interactions between the CNT sidewall or graphene and the adsorbates nonetheless changes its density of states (DOS) [58, 60–62], and has measurable impact on the conductivity of CNTs [59, 63]. This local interaction resulting from π -d orbital coupling has been correlated to an increase in the DOS of graphene which caused a drop in contact resistivity [64]. Further, adsorbates from the atmosphere such as H_2O , O_2 , CO_2 , and hydrocarbons, or from suspension solutions such as those used in drop-casting, can be trapped on the surface leading to the formation of a detrimental interfacial layer

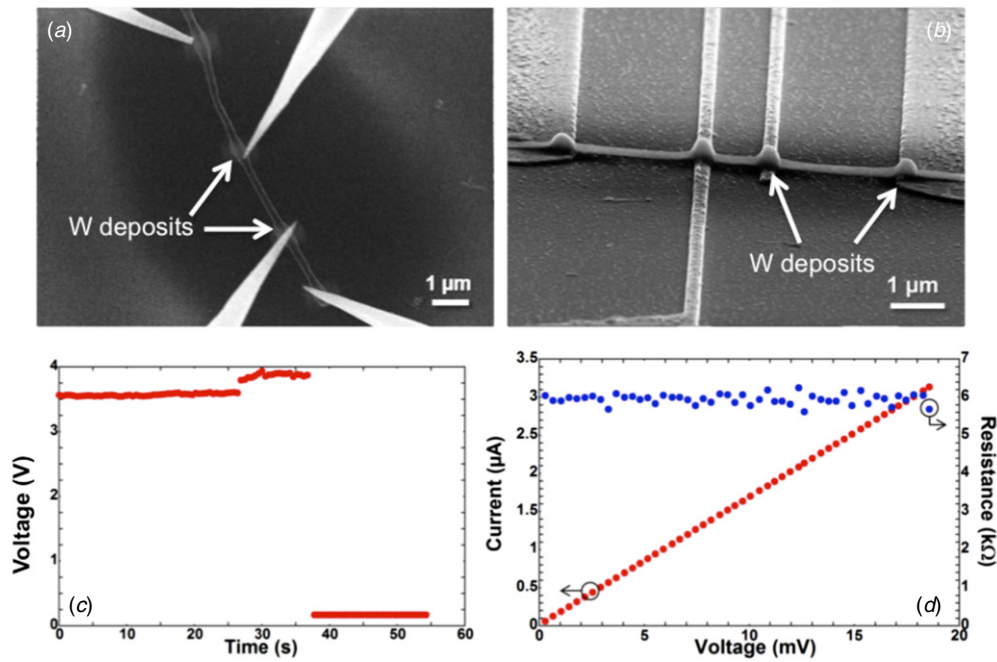


Figure 4. Configurations for 4PP measurements. (a) Directly probed drop-casted CNT on SiO₂ with EBID-W deposit on each contact. (b) CNT across pre-patterned pads each with EBID-W deposit. (c) Behavior upon voltage applied between outermost electrodes in configuration (a) under constant current of 100 µA. An abrupt drop at 37 s shows a significant resistance decrease attributed to the contact resistance reduction. (d) *I*–*V* characteristics for 4PP voltage between the inner electrodes show constant resistance. Similar results are obtained for configuration (b).

between the CNT sidewall and the metal electrodes, resulting in high contact resistance. It is likely that Joule heating by current stressing or contact improvement by rapid thermal annealing (RTA) in inert environments can lead to desorption of trapped chemical species [49, 63, 65], but their effect on contact resistance has not been fully assessed.

4PP measurements of CNTs during current stressing serve as an effective verification that the total device resistance reduction is due to changes at or near the metal–CNT interface [66, 67]. Two types of 4PP measurements have been employed by our group. A nanoprobe consisting of four piezo-actuated fingers is used inside an SEM to perform *in situ* measurements. Each finger has a tungsten tip with radii ≤ 50 nm that allows (1) direct probing of a drop-casted CNT and (2) probing of a patterned structure with deposited CNT contacts. Direct probing is hindered by the difficulty in making stable ohmic contact on the CNT surface due to radial deformations when pressure is applied. Additionally, drop-casting CNTs on pre-patterned electrodes rarely results in stable ohmic contact, which is required for the high-impedance voltage probes. To circumvent this problem, tungsten (W) was deposited on the contact areas using EBID to ensure an ohmic behavior for direct probing, as shown in figures 4(a) and (b). *I*–*V* curves from current stressing with 2PP and 4PP show that stressing between the outermost electrodes reduces the resistance between these contacts, while the resistance between the inner electrodes stays constant in either configuration up to 400 µA (figures 4(c) and (d)), when the CNT breaks down. The results clearly indicate that current stressing affects only the contacts, but not the CNT. It was reported that resistances of CNT devices with low contact resistance (0.5–5 kΩ) obtained

from either 2PP or 4PP measurements have little temperature dependence [67]. On the other hand, those with high contact resistances show significant decrease in device resistance with increasing temperature from 2PP measurements, while resistances from 4PP measurements shows little temperature dependence [67]. This is indicative of thermal activation of carriers across a non-ohmic (tunneling) junction at the metal–CNT interface [49], which is consistent with device resistance reduction by Joule heating due to contact improvement.

Another consideration is the metal–CNT contact area, since it leads to some degree of controllability in engineering the interface. A larger contact area clearly leads to a lower contact resistance. Based on calculations using DFT, it was suggested that weak metal–CNT hybridization with a large contact length could yield an optimum contact [68]. 2PP measurements on very long CNTs were used to determine an effective contact length (proportional to contact area) at which the resistance reached a minimum [38, 69], indicating a minimum contact length above which the total resistance is contact-area independent, as shown in figure 5. A semi-empirical model based on contact geometry was then used to extrapolate the resistivity of the CNTs and contact resistivity using Ti/Au electrodes [38, 69].

Apart from current stressing, a widely used contact engineering approach utilizes metal deposition by EBID or IBID. Such techniques can be applied as the sole means to fabricate the contact electrode, or to improve the metal–CNT interface of an existing device such as a drop-casted one. Generally, photolithography and electron beam lithography are used to form metal contacts [70]. These techniques provide good contacts for CNT transport measurements, but they

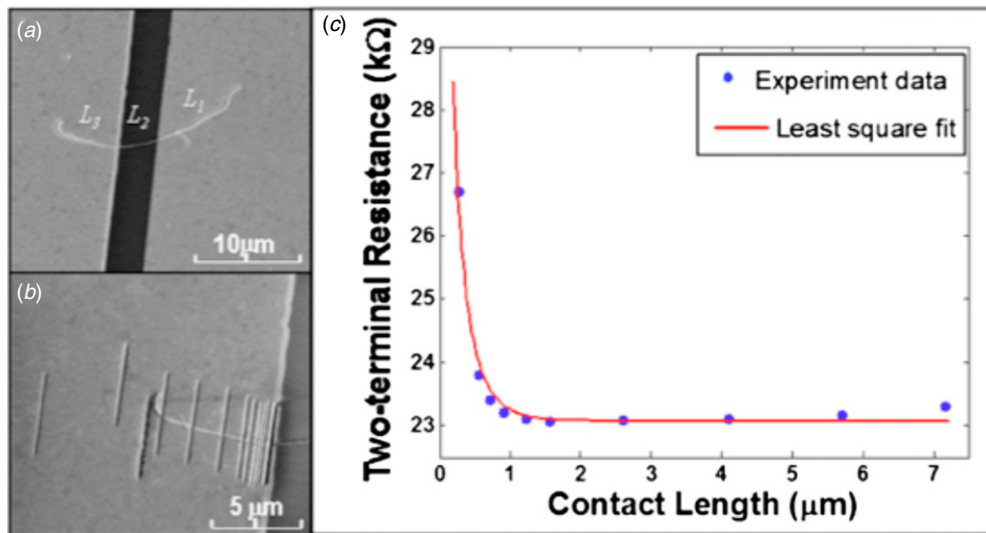


Figure 5. SEM images and data obtained from a typical MWCNT sample. (a) Image of MWCNT with two Ag thin film contacts before any FIB cuts were made. The Ag contacts covering both ends of the MWCNT are evident. (b) Same MWCNT after nine FIB cuts were completed. (c) Resistance versus contact length obtained after each cut. Resistance includes both the contact resistance and the MWCNT resistance of the $4 \mu\text{m}$ section of the MWCNT covered by Ag. Solid line is the best fit to the data which yield CNT resistivity $\rho_{\text{CNT}} = 4.70 \text{ k}\Omega \mu\text{m}$ and contact resistivity per unit length $\rho_{\text{C}} = 1.6 \text{ k}\Omega \mu\text{m}$. Reprinted with permission from the authors of [38]. Copyright 2008, AIP Publishing LLC.

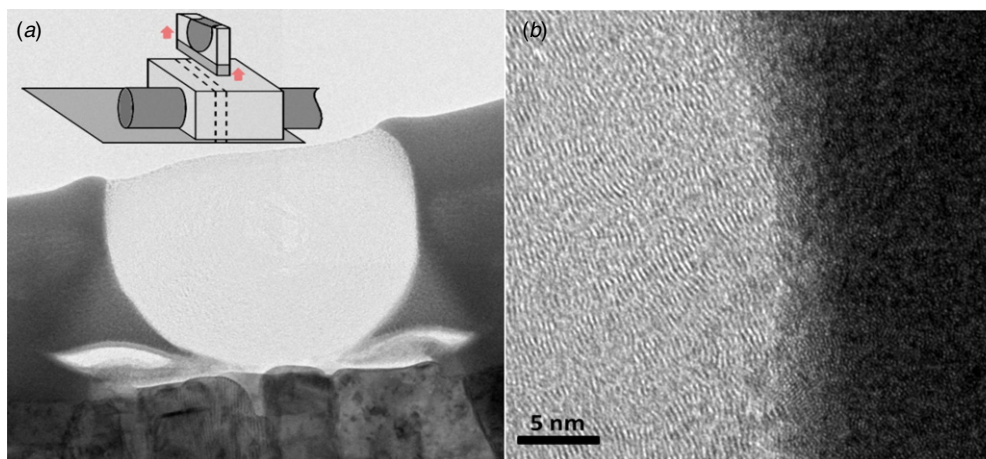


Figure 6. (a) Bright-field TEM cross-sectional view of CNT–Au–W electrode contact obtained by IBID–W deposition, with inset showing a schematic of the contact region and the ultra-thin slice from which the image was obtained. Voids at the intersection of all three materials are present as a result of the CNT shadow during W deposition. (b) High-resolution image of the IBID–W contact shows a clean interface with CNT.

require long sample preparation times. Alternatively, contacts can be formed by IBID using a focused ion beam (FIB) [19] and by EBID with an electron beam from a SEM [49]. Although neither technique leads to a scalable solution for integrating CNTs on-chip, they offer a versatile means for assessing the viability of these devices for next-generation interconnect applications.

Numerous metals can be deposited with IBID or EBID as long as a suitable source gas is available [71]. Recent results have suggested that graphitized C could yield the lowest contact resistance for interfacing with CNT interconnects [50, 72]. Chai *et al* [72] used electron beam evaporation to form metal contacts to a CNT using a technique reported earlier [73], yielding a lower resistance. Metal EBID has

been reported since 1960 [74], and has received much attention in recent years [75–82] for various applications such as etching and deposition [77], nanowire fabrication [78], and preparing tips for field emission [81] and atomic force microscope probes [82]. IBID–W is well known and frequently used for similar applications, and has been used extensively by our and other groups for making ohmic contacts with CNTs [19, 83–86]. IBID–W is generally more effective in reducing the contact resistance, but EBID–W produces similar contact resistance reductions, which can be further improved by current stressing. The W–CNT interface for a typical IBID–W deposited contact is shown in figure 6. Recent high-frequency two-port measurements on CNT test devices revealed a significant frequency-dependent capacitive

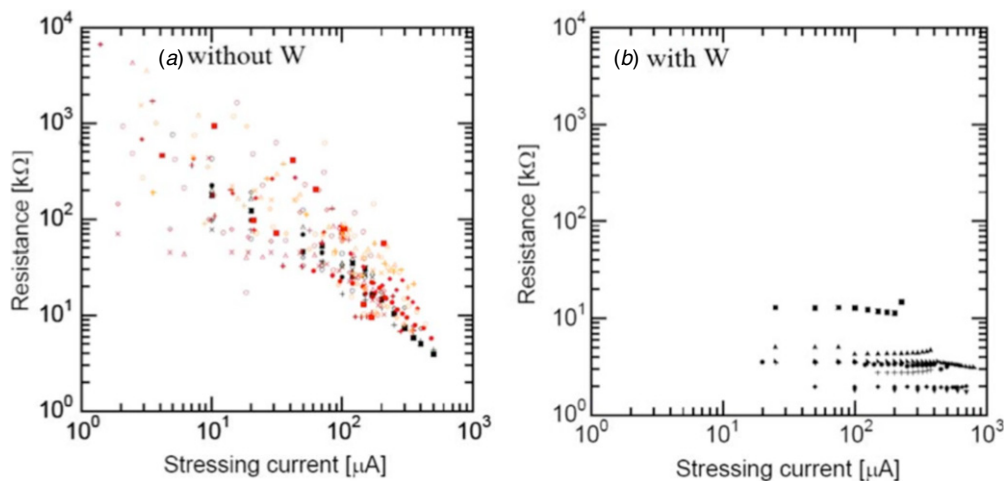


Figure 7. Resistance of two-terminal CNF test devices versus stress current (a) without W and (b) with IBID-W deposited on CNF/Au electrode contacts. Reprinted with permission from the authors of [19]. Copyright 2008, AIP Publishing LLC.

component in the large contact impedance for drop-casted contacts. Upon contact metallization with separately IBID-Pt and IBID-W and further current stressing, the contact impedance decreased drastically and became frequency-independent as well as virtually resistive, with a negligible reactive component [85, 86].

It should be noted that unlike IBID-W, the EBID-W deposits are likely to undergo changes in its crystallinity as well as chemical composition upon current stressing, which can contribute to further contact resistance reduction [71, 87]. Similarly, the relatively lower (and constant) resistance for devices with IBID-W deposited contacts is attributed to the higher degree of crystallinity as well as purity in the as-deposited W. Despite the higher purity of IBID-W deposit, it contains a significant amount of Ga which is undesirable for chip processing, and the IBID process does not seem to offer other significant advantages over EBID. Figure 7 shows the total resistance of a horizontal CNF interconnect test device versus applied stress current. The benefits of depositing W on the contacts are evident, especially for the case of IBID-W which show low resistance that remains invariant under current stressing, suggesting that the contact resistance is minimized [19]. While these results are particular to W, the technique is applicable to other metals, and the final resistance value may be lower for metals with matching work functions to that of CNT and higher wettability [36].

Despite progress made in contact engineering to improve side-contacted metal–CNT interfaces, further improvements are critically needed for CNTs to be incorporated in functional devices. Table 1 summarizes the results reported in the literature for side-contacted CNT structures. As reported by numerous groups including ours, the better way to make metal–CNT contacts is to bind the metal surface atoms to the unsaturated C-bonds at the edge of the graphene wall, namely, making end contacts [50]. This configuration is discussed in the next section in conjunction with delineation between the as-grown metal–CNT interface and that formed by metal deposition.

3. End-contacted structures

For vertically aligned CNTs, it is natural to make end contacts at the as-grown interface with the metal underlayer, yielding lower contact resistance than that for side-contacted CNTs. Figure 8 shows a series of cross-sectional TEM images of metal–CNT (CNF in this case) interfaces grown on a Ti underlayer using plasma-enhanced chemical vapor deposition (PECVD). The interface regions display little evidence of impurities, and clearly show the graphitic planes nearly normal to the metal surface. From these images, it appears that the graphitic planes make direct contact to the Ti surface atoms, providing the necessary bonding to facilitate carrier transport and resulting in low contact resistance. While formation of carbides at this interface have been reported [88–90], it is unclear if this occurs for all PECVD-grown CNTs. Generally when the wettability between the CNT and the metal underlayer is high, such as that for Ti or Cr, which correlates with strong bonding between carbon and metal surface atoms (see figure 3(c)), it is likely that metal carbide may form at the interface. A comparison of side-contacted and end-contacted CNTs with interfacial tungsten carbide formed by electron beam irradiation was made, which showed significantly more reduction in resistance for the end-contacted device [90]. Similar results have been observed [50] or predicted [91], if contact areas are taken into account. Very recently, Wang *et al* [92] reported a contact geometry in which only the 1D edge of a graphene layer was metallized. This has noticeable impact on graphene performance, drastically reducing contact resistance and improving carrier mobility [92]. In the case of SWCNTs [52], the interface with metal occurs with one single graphene shell and may be insensitive to contact geometry if the side-contacted area is sufficiently large. In the case of end-contacted vertically aligned MWCNTs [53], if the as-grown and/or top contact were poor, then the total contact resistance would be similar to that for side contact with a larger contact area. In general, end-contacted geometries are advantageous over side contacts because of the absence of an interfacial layer or gap across which carrier tunneling occurs, as described in the previous section.

Table 1. Summary of reported results for side-contacted CNT structures, where R_T , R_{CNT} , ρ_{CNT} , and R_C are total resistance, CNT resistance, CNT resistivity, and contact resistance, respectively.

Reference	Year	Structure	Electrodes	R_T (k Ω)	R_{CNT} (k Ω)	ρ_{CNT} (k $\Omega \mu\text{m}$)	R_C (k Ω)	Notes
[50]	2012	MWCNT	Au/Graphite	26.5				EBID-C with J heating, single shell contact. Contact graphitized
[84]	2012	MWCNT	Au/W Au/W/CNT			1–10	>50 k $\Omega \mu\text{m}$	Value for MWCNT–MWCNT contact. For MWCNT with Au, $R_C > 100 \text{ k}\Omega \mu\text{m}$
[104]	2011	MWCNT	TiN/CNT	25–80				metal–CNT–CNT–metal contact.
[104]	2011	MWCNT	TiN	50–220	50			metal–CNT–metal
[90]	2010	MWCNT	W	10.2				Two-terminal side-contact MWCNT to W electrode, e-beam induced joule heating at contact to form W-Carbide
[52]	2009	SWCNT	Pt	50–80				No difference between side contact and end contact.
[73]	2009	SWCNT	Pt	4.8×10^1 – 4.6×10^3			>25	Individual SWNTs. Annealing in inert atmospheres drastically reduces R_C and graphitizes contacts with Pt.
[19]	2008	CNF	Au	6.0 – 1×10^6				Contact resistance reduction improved by stress currents
[19]	2008	CNF	Au/W	1.0–10				Contact resistance improved by IBID-W, invariant to stress currents
[69]	2008	MWCNT	Ti/Au			0.33–1.48	1–5 k $\Omega \mu\text{m}$	Semi-empirical estimates
[55]	2007	SWCNT	Pt	826–152				R_C reduced by Joule heating through current stressing
[66]	2006	MWCNT	Pt/Au	~70	~70		3–4	4PP measurement
[66]	2006	SWCNT bundle	Pt/Au	~100	~100		5	4PP measurement
[70]	2004	CNF	Ti/Au			3.2×10^{-2} – 4.2×10^{-2}	~ 1 k Ω range	4PP measurement
[98]	2003	MWCNT	Au, Pd	2.5×10^3 – 20×10^3				CNT with Au and Pd electrodes. 4PP measurements
[98]	2003	MWCNT	Co	~20–100				CNT with Co electrodes. 4PP measurements
[98]	2003	MWCNT	Au/Ni	~20–200				Ni deposited on CNT contacts with Au. 4PP measurements
[98]	2003	MWCNT	Pd/Ni	~20–80				Ni deposited on CNT contacts with Pd. 4PP measurements
[98]	2003	MWCNT	Co/Ni	~20–120				Ni deposited on CNT contacts with Co. 4PP measurements
[27]	2003	MWCNT	Ti/Au	3.0×10^1 – 8.8×10^3				Early work on side-contacted MWCNT
[83]	2001	MWCNT	W	2.4	1.7		0.7	MWCNT with IBID-W (4PP) current stressing $>10^9 \text{ A cm}^{-2}$. Assert W contacts ~100 Ω
[67]	2000	MWCNT	Ti/Au		~10–20		0.5–50	Drastic reduction of R_C after RTA. 4PP measurements
[105]	1999	SWCNT	Ti/Au	250–16.5				Individual SWCNT temperature-dependent two-terminal resistance measurements
[47]	1998	MWCNT	Au, Au/C		0.35–2.6		4–30	First paper of drastic R_C reduction by carbon deposition at contacts

The top contact of an as-grown CNT is likely to behave differently from the as-grown or base contact. As shown in figure 8, there is a Ni catalyst particle embedded in each CNT tip, a characteristic of the so-called tip growth common for most nanotubes and nanowires. Without further processing, the interface between such CNT tip and metal can be problematic for certain applications where compatibility of catalyst with fabrication process may prove deleterious. Upon suitable polishing and removal of the catalyst particle at the tip [93], the

top edge of each CNT is likely to consist of unsaturated carbon bonds, making it susceptible to react with the environment and to contamination. Thus proper procedures must be performed to produce a top metal–CNT interface that would not add significantly to the overall contact resistance. The merit of removing the catalyst tip to improve contact resistance depends on the methods and materials used to pattern the top electrode. In particular, if the top electrode material has better wetting characteristics to catalyst than CNT, leaving the catalyst intact

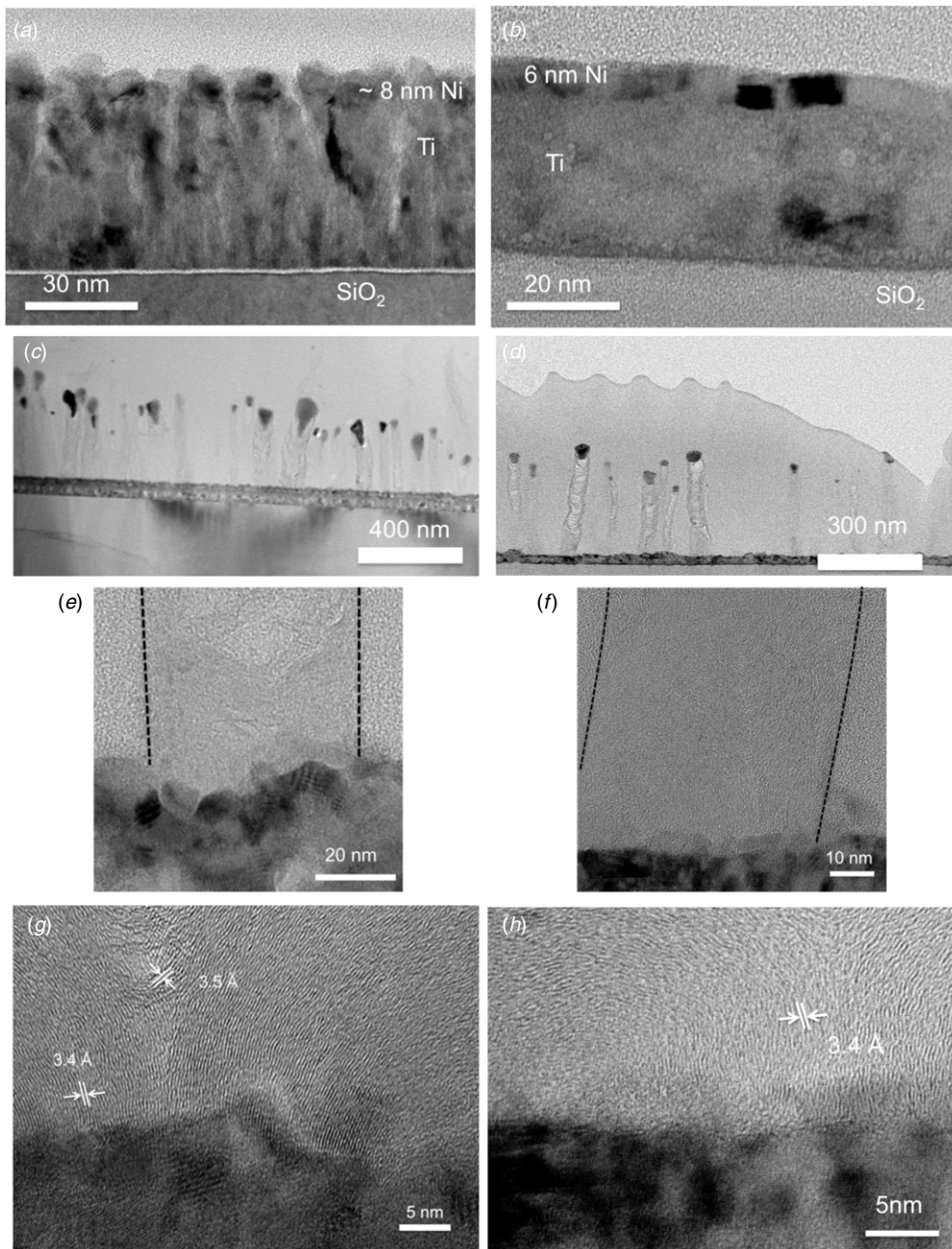


Figure 8. Comparison between two similar catalyst/underlayer metal structures deposited by magnetron sputtering with (a) $<10^{-6}$ torr base pressure, 100W DC and (b) $<10^{-8}$ torr base pressure, 100 W RF. The resulting CNFs grown at the same time for each sample have significant different structures with (c) cup-shape CNF morphology and (d) bamboo-shape CNF morphology. Interfacial images show clean contacts (e) and (f). (g) and (h) Interfaces showing graphitic interplanar spacing, and graphene planes nearly normal to the underlayer metal surface.

may result in decreased contact resistance. On the other hand, if removing the catalyst particle can improve the top electrode–CNT contact resistance compared with that formed directly on the catalyst particle, surface pre-treatment using plasma [51, 70] and post-treatments such as annealing [44, 50, 55, 67, 73] should be considered.

Despite the many known facts about CNTs grown using CVD and PECVD [94, 95], interface nanostructure versus electrical property relationships have not been studied in sufficient depth that can lead to consistent control and reduction of contact resistance. It has been reported that metals

with high wettability (Ti, Cr, and Fe) could provide the lowest contact resistances, whereas when the wettability is low, the contact resistance is strongly correlated to the metal–CNT work-function difference [36]. Since low contact resistance is a necessity for high performance for CNT interconnects, parameters such as wettability and work function are more important than the resistivity of the contacting metal. To study this, dense CNT vias were grown on a Ti underlayer, and then patterned with a variety of different metals, as shown in figure 9 [36]. While work-function matching correlates to lower contact resistance, metals with outer d-orbital vacancies

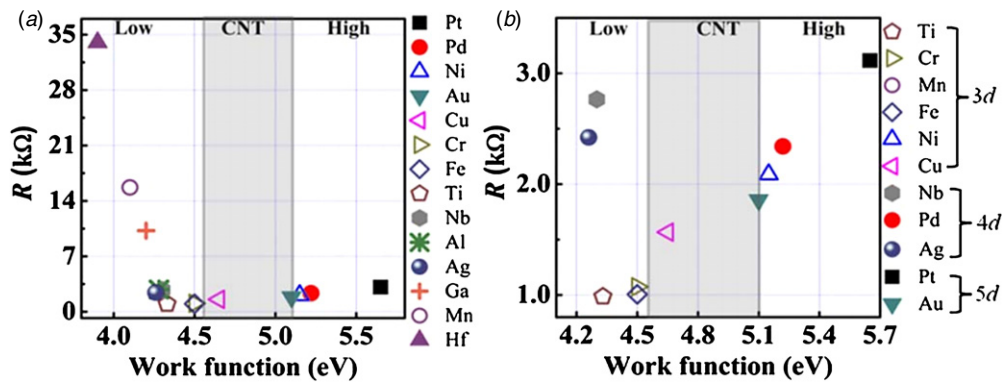


Figure 9. (a) Metal-CNT contact resistance versus metal work function. (b) Contact resistance versus work function behaviors for metals with work functions between 4.2 and 5.7 eV highlights the relationship between unoccupied d-orbitals and contact resistance. CNT work function range is shaded. Lower resistance correlates with work-function matching and higher number of unoccupied d-orbitals, but higher wettabilities do not necessarily follow from small work function difference. Reprinted with permission from the authors of [36]. Copyright 2009, AIP Publishing LLC.

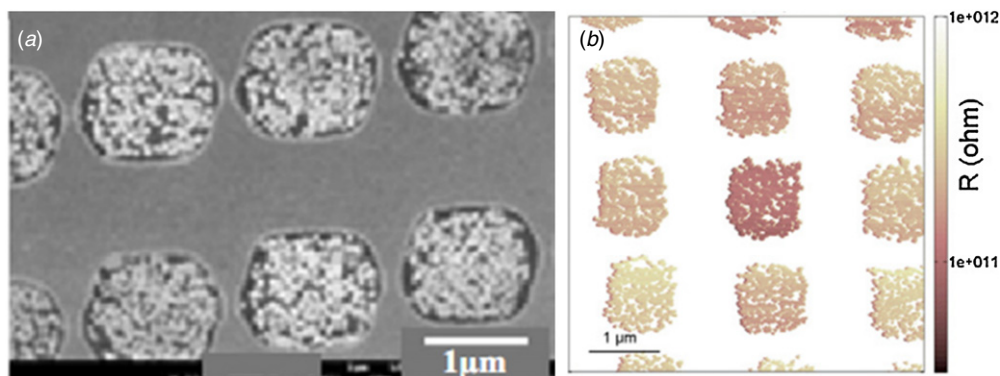


Figure 10. (a) SEM image of fabricated CNT vias. (b) Scanning spreading resistance map for fabricated CNT vias. Reprinted from [100]. Copyright 2011, with permission from Elsevier.

achieve the lowest resistance and they are known to have higher wettabilities [96, 97]. The authors also reported that metal-CNT junctions with poor wettability result in barrier formation where conduction is governed by tunneling, hence the role of work-function difference becomes dominant. The effect of d-orbital vacancies has been observed for Co-CNT contacts, which yielded much lower measured total resistance than Au or Pd ones, as Co is a transition metal with three unoccupied d-orbitals [98].

In a vertical configuration, where each individual CNT or CNT array is usually embedded in an insulator for electrical probing, 4PP measurements would require an elaborate test structure, which is not only challenging to design and fabricate but could also change the inherent materials and interface characteristics of the test device. Thus, two-terminal measurements are generally used in conjunction with a transmission line model to extract resistance using scanning probe [45, 99, 100] and fixed-probe techniques [44, 99]. Scanning probe techniques such as one using an atomic force microscope (AFM) with a biased tip, allow direct probing of individual CNTs, as shown in figure 10 [100]. However, because the tip is actively scanning during each measurement, it is usually performed at low fixed voltages and low currents. While the probe can be affixed over an individual CNT for an I - V scan, it precludes the ability to use sufficiently high current density to reduce the contact resistance between the

CNT and the AFM tip, and typically results in high measured resistances [45, 46, 100]. When the measurement is performed in static mode, there is uncertainty in probe positioning, as the contact between the CNT and the probe can change without any feedback to the user. In scanning mode (fixed bias), there is uncertainty whether sufficient pressure is applied to produce good ohmic contact. On the other hand, fixed-probe techniques, such as one using a wafer probe station with an optical microscope, have too low a spatial resolution to land a probe over a single CNT. Thus, resistance of the entire CNT array or bundle is usually measured using such techniques, as given in the summary of reported results for end-contacted structures in table 2. A via with densely-packed CNTs that is patterned with a sufficiently large pitch (via-to-via separation) such that a probe can land on a single via device, can lend itself well to this technique. In this case, measurements of the total via resistance may be the only metric that is meaningful for device integration, and focus is placed on fabrication and integration of CNT vias into the overall process flow [53, 54, 99, 101]. Using this approach, two-terminal measurements of 160 nm CNT vias yielded a total resistance value of just 34 Ω per via with a CNT packing density of $3 \times 10^{11} \text{ cm}^{-2}$, as shown in figure 11 [54]. In this case, the interstitial spacing among CNTs inside each via was filled with spin-on glass. The encapsulation material has been found to play an important role in electrical conduction in CNT vias,

Table 2. Summary of reported results for end-contacted CNT structures, where R_T , R_{CNT} , ρ_{CNT} , and R_C are total resistance, CNT resistance, CNT resistivity, and contact resistance, respectively.

Reference	Year	Structure	Electrodes (Bottom/Top)	Via dimensions ($W \times H$) nm	CNT Count or density (# or cm^{-2})	R_T (k Ω)	ρ_{CNT} (k $\Omega \mu\text{m}$)	R_C (k Ω)	Notes
Present work		CNF	Ti/W		1		1.7×10^{-3} – 2.4×10^{-3}	0.570–0.230	Film quality affects resistivity and contact resistance. Extrapolated by variable height measurements
[51]	2013	CNT bundle	Pd/Au \times 2				2.7	0.29/contact	End-bonded
[51]	2013	CNT bundle	Pd/Au \times 2				1.8	1.8/contact	Wrap-around
[51]	2013	CNT bundle	Cr/Al \times 2				3.5	0.29/contact	End-bonded
[51]	2013	CNT bundle	Pd/Au \times 2				2.4	0.29/contact	Wrap-around
[51]	2013	CNT bundle	Cr/Al \times 2				3.2	0.29/contact	End-bonded
[51]	2013	CNT bundle	Pd/Au \times 2				1.6	0.29/contact	Wrap-around
[50]	2012	MWCNT	(Au/graphite)/ (Au/graphite)			0.116			EBID-C with J heating, multiple shell contact. Contact graphitized
[53]	2011	MWCNT via	TiAu/TiN	$300 \times (250\text{--}550)$	~ 100	$\sim 4\text{--}8$	$< 1.39 \times 10^{-3}$	1.6 per via, 116 per tube (avg.)	Variable height extrapolation
[99]	2011	MWCNT forest	CoSi ₂ /AFM tip		1	140–20			Two-terminal C-AFM
[101]	2011	MWCNT Via	TiAu/TiN	80×250	$3.50 \times 10^{11} \text{ cm}^{-2}$	0.493–0.293			Via resistance decreased from k Ω after thermal annealing
[100]	2011	MWCNT Via	Poly Si/AFM tip		1.5×10^{12}	$> \text{G}\Omega$			Scanning spreading resistance shows color representation of individual resistance
[44]	2010	CNF	Ti/W		1		4.6×10^{-3}	4.2	Extrapolated by variable height measurements
[44]	2010	CNF	Cr/W		1		1.2×10^{-2}	5.0	Extrapolated by variable height measurements
[90]	2010	MWCNT	W-C/W-C		1	0.710			Two-terminal end-contact MWCNT to W electrode, e-beam induced joule heating at contact to form W-Carbide
[46]	2010	CNF	Ti/W		1			1.8	Fe-catalyzed CNF on Ti Extrapolated by variable height measurements
[46]	2010	CNF	Cr/W		1			3.8	Fe-catalyzed CNF on Cr Extrapolated by variable height measurements
[36]	2009	m- and s-CNT array	Ti/(Pt, Pd, Ni, Au, Cu, Cr, Fe, Ti, Nb, Al, Ag, Ga, Mn or Hf)	$200 \times \sim 150$				1–35 for top electrode	Contact resistance estimated over a large average. Figure 9.
[45]	2009	CNF	Ti/Pt (AFM tip)		1		7.3×10^{-3}	6.4	Two-terminal C-AFM
[54]	2008	MWCNT Via	(Cu/TaN/Ta/TiN)/TiCu	160×120	3×10^{11}	0.063–0.034			Low temperature growth for CMOS process compatibility

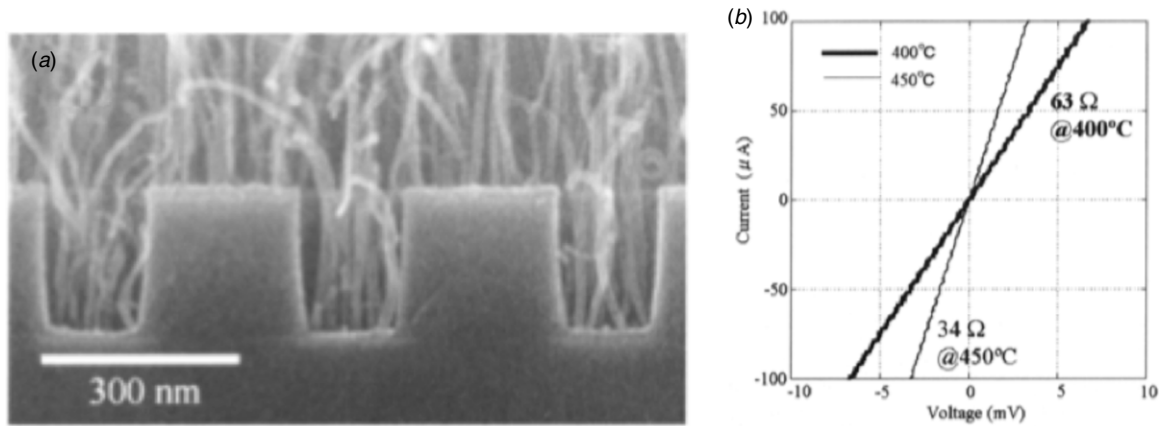


Figure 11. 160 nm-diameter CNT via after growth and before polish and electrode patterning. (b) Resistance measurements for CNT via grown at 400 and 450 °C. The difference in resistance was attributed to difference in CNT quality for the two growth temperatures. Copyright 2008, IEEE. Reprinted with permission from the authors of [54].

where Al_2O_3 deposited by atomic layer deposition was found to increase the via resistance by a factor of three compared with SiO_2 deposited by thermal decomposition of TEOS [99, 102]. It is worthwhile to note that encapsulation with Cu in a metal–CNT composite via could yield lower resistance values while retaining the high current capacity of CNT [103]. Table 2 summarizes reported results for end-contacted CNT structures.

A nanomanipulating probe installed inside an electron microscope is suitable for performing *in situ* two-terminal measurements on individual CNTs. Contact resistance extraction for individual vertically aligned CNTs with various heights (or lengths) and similar diameters has been performed using a statistical linear regression technique [44]. In this case, the measured total device resistance is assumed to vary with only the CNT length, as given below:

$$R_{\text{Total}} = R_C + R_{\text{CNT}} = R_C + \frac{4\rho}{\pi D_{\text{CNT}}^2} L_{\text{CNT}}. \quad (1)$$

R_C represents the total contact resistance (including top and base contacts), ρ is the CNT resistivity, and L_{CNT} and D_{CNT} are the measured CNT length and diameter, respectively. This method is based on limiting the CNT diameter values to a narrow window, thus validating the constant-diameter assumption, and on the further assumption that the contact resistance for each CNT in the array is invariant for a given diameter value. By measuring CNTs with varying lengths, the resistivity and contact resistance were extracted. Additionally, each CNT was current-stressed to reduce the contact resistance between the CNT and the probe, since these devices display similar nonlinear I – V characteristics as side-contacted CNTs upon initially landing the probe. For a similar configuration using W tips as electrodes, Joule heating through high-energy electron radiation at the interface between the W tip and a single CNT resulted in tungsten carbide formation and a total resistance of 710 Ω [90].

The complex relationships among the underlayer metal, CNT catalyst, and CNT growth conditions are far from being well understood, but they nonetheless play a critical role in determining the metal–CNT contact resistance, as well as the CNT array density [46]. For high CNT density, low wettability

between the catalyst and the underlayer metal was suggested, at least in cases where catalyst patterning is performed with film depositions prior to growth [46], whereas for low contact resistance, high wettability between the resulting CNT and the underlayer metal was proposed [36]. Thus to obtain higher CNT array density and hence lower contact resistance, the catalyst/underlayer metal as well as the CNT/underlayer metal wettabilities must be considered. Further, process controls that impact the quality (crystallinity and purity) of the deposited underlayer metal and catalyst prior to CNT growth have not been systematically studied and can also impact the contact resistance, as suggested by the interface images shown in figure 8. Both structures were grown simultaneously under identical conditions, and have similar Ni catalyst film thicknesses on a relatively thick Ti underlayers. However, the resulting Ti/Ni interfaces from different deposition conditions yielded dissimilar CNT structures and contact resistances. In both cases, the metals were deposited without breaking vacuum, although the base pressure for depositing the structure in figure 8(a) was 10^{-6} and 10^{-9} torr for the other. The same technique described earlier [44] was used to extract the contact resistance using equation (1), yielding results shown in figure 12. The contact resistance is fairly low in either case, but it is necessary to take into account the measurement configuration and examine further the extracted value, which consists of the following components:

$$R_C \equiv R_{\text{bundle}} + R_m + R_{\text{CNT}/m} + R_{p/\text{CNT}}. \quad (2)$$

Upon extracting the resistance contributions from the CNT bundle (R_{bundle}) serving as one electrode and the underlayer metal (R_m), the remaining or true contact resistance [$R_{\text{CNT}/m}$ (as-grown contact) + $R_{p/\text{CNT}}$ (probe–CNT contact)] has values of $\sim 570 \Omega$ for the device corresponding to the structure in figure 8(a) and $\sim 230 \Omega$ for the one in figure 8(b). Decoupling the two components in the true contact resistance is not possible for our measurement configuration. We surmise that the as-grown interface (Ti–CNT) remains relatively invariant during current stressing, whereas the contact between the CNT and the W-probe is successively improved by increasing stress current, possibly leading to carbide formation as mentioned earlier [90].

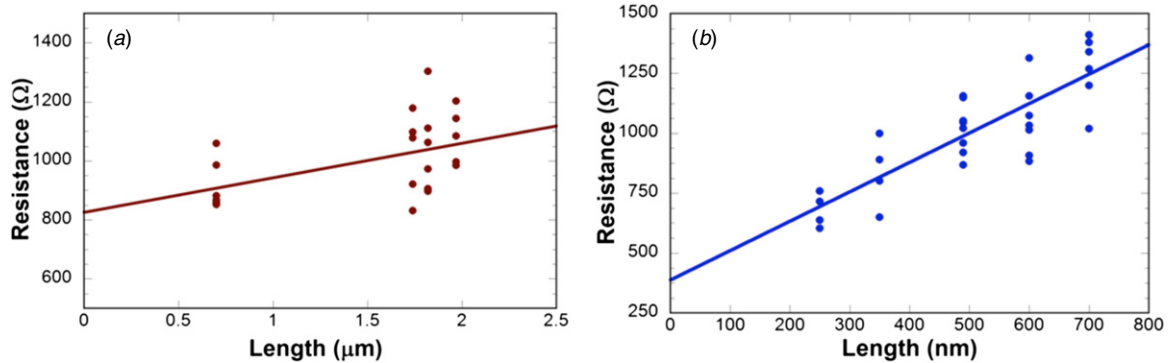


Figure 12. Extraction of resistivity and contact resistance for (a) CNTs grown on substrate shown in figure 8(a), and (b) those shown in figure 8(b).

4. Summary and conclusions

Before seriously considering CNT as a candidate for incorporation into IC technology, there remains significant concern whether high-performance CNT interconnects can be realized in a research environment. The primary issue continues to be high contact resistance arising from the metal–CNT interface. Contact engineering is progressing and results in sub-k Ω contact resistance values, which still need to decrease considerably before device functionalization. Contact resistance can be drastically reduced by Joule heating (current stressing, RTA, or electron beam irradiation) and through metallization of the contacts using selection criteria governed by the wettability between the metal and CNT and work-function difference. Methods for probing and extracting contact resistances can be performed even for vertical structures where 4PP is difficult if not impossible. End-contacted vertical structures typically result in lower contact resistance due in large part to strong bonding between edge carbon and surface metal atoms. And it is likely that the as-grown interface between a CNT and the underlayer metal can yield a very low contact resistance under the best growth conditions, such as catalyst and underlayer metal depositions without ambient adsorbates trapped at the interfaces. In a vertical configuration with a clean as-grown interface, the electrical conduction bottleneck is likely to be the as-deposited electrode or electrical probe. Although the contact resistance can be reduced by Joule heating in either contact geometry, it is worthwhile to perform surface pre-cleaning to remove adsorbates prior to metal depositions. With further progress made in CNT growth and contact engineering, it is entirely conceivable that the end-contacted CNT structure will soon yield a total via resistance comparable to that of Cu in the most advanced IC technology node.

References

- [1] Dresselhaus M S, Dresselhaus G and Eklund P C 1996 *Science of Fullerenes and Carbon Nanotubes: Their Properties and Applications* (New York: Academic)
- [2] Dresselhaus M S, Dresselhaus G and Avouris P 2001 *Carbon Nanotubes: Synthesis, Structure, Properties, and Applications* (Berlin: Springer)
- [3] Ijima S 1991 Helical microtubules of graphitic carbon *Nature* **354** 56–58
- [4] Dekker C 1999 Carbon nanotubes as molecular quantum wires *Phys. Today* **52** 22–28
- [5] Kreupl F, Graham A P, Duesberg G S, Steinhögl W, Liebau M, Unger E and Hönlein W 2002 Carbon nanotubes in interconnect applications *Microelectron. Eng.* **64** 399–408
- [6] Li J, Ye Q, Cassell A, Ng H T, Stevens R, Han J and Meyyappan M 2003 Bottom-up approach for carbon nanotube interconnects *Appl. Phys. Lett.* **82** 2491–3
- [7] Nihei M, Kawabata A, Kondo D, Horibe M, Sato S and Awano Y 2005 Electrical properties of carbon nanotube bundles for future via interconnects *Japan. J. Appl. Phys.* **44** 1626
- [8] Zhang L, Austin D, Merkulov V I, Meleshko A V, Klein K L, Guillorn M A, Lowndes D H and Simpson M L 2004 Four-probe charge transport measurements on individual vertically aligned carbon nanofibers *Appl. Phys. Lett.* **84** 3972–4
- [9] Melechko A V, Merkulov V I, McKnight T E, Guillorn M A, Klein K L, Lowndes D H and Simpson M L 2005 Vertically aligned carbon nanofibers and related structures: controlled synthesis and directed assembly *J. Appl. Phys.* **97** 041301
- [10] Ngo Q, Yamada T, Suzuki M, Ominami Y, Cassell A M, Jun L, Meyyappan M and Yang C Y 2007 Structural and electrical characterization of carbon nanofibers for interconnect via applications *IEEE Trans. Nanotechnol.* **6** 688–95
- [11] Geim A K and Novoselov K S 2007 The rise of graphene *Nature Mater.* **6** 183–91
- [12] Moon J S et al 2009 Epitaxial-graphene RF field-effect transistors on Si-face 6H-SiC substrates *IEEE Electron Device Lett.* **30** 650–2
- [13] Bae S et al 2010 Roll-to-roll production of 30-inch graphene films for transparent electrodes *Nature Nanotechnol.* **5** 574–8
- [14] Moon J S, Curtis D, Bui S, Marshall T, Wheeler D, Valles I, Kim S, Wang E, Weng X and Fanton M 2010 Top-gated graphene field-effect transistors using graphene on Si (111) wafers *IEEE Electron Device Lett.* **31** 1193–5
- [15] Naeemi A and Meindl J D 2009 Carbon nanotube interconnects *Annu. Rev. Mater. Res.* **39** 255–75
- [16] Pop E, Mann D, Cao J, Wang Q, Goodson K and Dai H 2005 *Phys. Rev. Lett.* **95** 155505
- [17] Li H, Xu C and Banerjee K 2010 Carbon nanomaterials: the ideal interconnect technology for next-generation ICs *IEEE Des. Test Comput.* **27** 20–31
- [18] De Volder M F L, Tawfik S H, Baughman R H and Hart A J 2013 Carbon nanotubes: present and future commercial applications *Science* **339** 535–9
- [19] Kitsuki H, Yamada T, Fabris D, Jameson J R, Wilhite P, Suzuki M and Yang C Y 2008 Length dependence of current-induced breakdown in carbon nanofiber interconnects *Appl. Phys. Lett.* **92** 173110

- [19] Saito T, Yamada T, Fabris D, Kitsuki H, Wilhite P, Suzuki M and Yang C Y 2008 Improved contact for thermal and electrical transport in carbon nanofiber interconnects *Appl. Phys. Lett.* **93** 102108
- [20] Yamada T, Saito T, Fabris D and Yang C Y 2009 Electrothermal analysis of breakdown in carbon nanofiber interconnects *IEEE Electron Device Lett.* **30** 469–71
- [21] Suzuki M, Yamada T and Yang C Y 2007 Monte Carlo simulation of scanning electron microscopy bright contrast images of suspended carbon nanofibers *Appl. Phys. Lett.* **90** 083111
- [22] Yamada T, Madriz F R and Yang C Y 2009 Inductance in one-dimensional nanostructures *IEEE Trans. Electron Devices* **56** 1834–9
- [23] Yamada T, Yabutani H, Saito T and Yang C Y 2010 Temperature dependence of carbon nanofiber resistance” *Nanotechnology* **21** 265707
- [24] ITRS 2011 International technology roadmap for semiconductors www.itrs.net/Links/2012ITRS/Home2012.htm (with 2012 updates)
- [25] Wang T, Jeppson K, Olofsson N, Campbell E E and Liu J 2009 Through silicon vias filled with planarized carbon nanotube bundles *Nanotechnology* **20** 485203
- [26] Knickerbocker J U et al 2006 3-D silicon integration and silicon packaging technology using silicon through-vias *IEEE J. Solid-State Circuits* **41** 1718–25
- [27] Wakaya F, Katayama K and Gamo K 2003 Contact resistance of multiwall carbon nanotubes *Microelectron. Eng.* **67** 853–7
- [28] Berger H H 1972 Models for contacts to planar devices *Solid-State Electron.* **15** 145–58
- [29] Lundstrom M and Ren Z 2002 Essential physics of carrier transport in nanoscale MOSFETs *IEEE Trans. Electron Devices* **49** 133–41
- [30] Kondo D, Sato S and Awano Y 2008 Self-organization of novel carbon composite structure: graphene multi-layers combined perpendicularly with aligned carbon nanotubes *Appl. Phys. Express* **1** 074003
- [31] Nihei M, Kondo D, Kawabata A, Sato S, Shioya H, Sakaue M, Iwai T, Ohfuti M and Awano Y 2005 Low-resistance multi-walled carbon nanotube vias with parallel channel conduction of inner shells *Proc. IEEE Int. Interconnect Technology Conf.* pp 234–6
- [32] Naeemi A and Meindl J D 2008 Design and performance modeling for single-walled carbon nanotubes as local, semiglobal, and global interconnects in gigascale integrated systems *IEEE Trans. Electron Devices* **54** 26–37
- [33] Nagashio K, Nishimura T, Kita K and Toriumi A 2009 Metal/graphene contact as a performance killer of ultra-high mobility graphene analysis of intrinsic mobility and contact resistance *IEDM'09: IEEE Int. Electron Devices Meeting* pp 1–4
- [34] Venugopal A, Colombo L and Vogel E M 2010 Contact resistance in few and multilayer graphene devices *Appl. Phys. Lett.* **96** 013512
- [35] Smith J T, Franklin A D, Farmer D B and Dimitrakopoulos C D 2013 Reducing contact resistance in graphene devices through contact area patterning *ACS Nano* **7** 3661–7
- [36] Lim S C, Jang J H, Bae D J, Han G H, Lee S, Yeo I S and Lee Y H 2009 Contact resistance between metal and carbon nanotube interconnects: effect of work function and wettability *Appl. Phys. Lett.* **95** 264103
- [37] Yamada T, Saito T, Suzuki M, Wilhite P, Sun X, Akhavantafi N, Fabris D and Yang C Y 2010 Tunneling between carbon nanofiber and gold electrodes *J. Appl. Phys.* **107** 044304
- [38] Lan C, Zakharov D N and Reifengerger R G 2008 Determining the optimal contact length for a metal/multiwalled carbon nanotube interconnect *Appl. Phys. Lett.* **92** 213112
- [39] Svensson J and Campbell E E 2011 Schottky barriers in carbon nanotube-metal contacts *J. Appl. Phys.* **110** 111101
- [40] Palacios J J, Pérez-Jiménez A J, Louis E, SanFabián E and Vergés J A 2003 First-principles phase-coherent transport in metallic nanotubes with realistic contacts *Phys. Rev. Lett.* **90** 106801
- [41] Kong J, Yenilmez E, Tomblor T W, Kim W and Dai H 2001 Quantum interference and ballistic transmission in nanotube electron waveguides *Phys. Rev. Lett.* **87** 106801
- [42] Matsuda Y, Deng W Q and Goddard W A 2007 Contact resistance properties between nanotubes and various metals from quantum mechanics *J. Phys. Chem. C* **111** 11113–6
- [43] Xia F, Perebeinos V, Lin Y-M, Wu Y and Avouris P 2011 The origins and limits of metal-graphene junction resistance *Nature Nanotechnol.* **6** 179–84
- [44] Li K, Wu R, Wilhite P, Khera V, Krishnan S, Sun X and Yang C Y 2010 Extraction of contact resistance in carbon nanofiber via interconnects with varying lengths *Appl. Phys. Lett.* **97** 253109
- [45] Wu W, Krishnan S, Yamada T, Sun X, Wilhite P, Wu R, Li K and Yang C Y 2009 Contact resistance in carbon nanostructure via interconnects *Appl. Phys. Lett.* **94** 163113
- [46] Sun X, Li K, Wu R, Wilhite P, Saito T, Gao J and Yang C Y 2010 The effect of catalysts and underlayer metals on the properties of PECVD-grown carbon nanostructures *Nanotechnology* **21** 045201
- [47] Bachtold A, Henny M, Terrier C, Strunk C, Schonenberger C, Salvetat J P, Bonard J M and Forro L 1998 Contacting carbon nanotubes selectively with low-ohmic contacts for four-probe electric measurements *Appl. Phys. Lett.* **73** 274–6
- [48] Brintlinger T, Fuhrer M S, Melngailis J, Utke I, Bret T, Perentes A, Hoffmann P, Abourida M and Doppelt P 2005 Electrodes for carbon nanotube devices by focused electron beam induced deposition of gold *J. Vac. Sci. Technol. B* **23** 3174–7
- [49] Maeda S, Wilhite P, Kanzaki N, Yamada T and Yang C Y 2011 Change in carbon nanofiber resistance from ambient to vacuum *AIP Adv.* **1** 022102
- [50] Kim S, Kulkarni D, Rykaczewski K, Henry M, Tsukruk V and Fedorov A 2012 Fabrication of an ultra-low-resistance ohmic contact to MWCNT-metal interconnect using graphitic carbon by electron beam induced deposition (EBID) *IEEE Trans. Nanotechnol.* **11** 1223–30
- [51] Chiodarelli N, Fournier A and Dijon J 2013 Impact of the contact’s geometry on the line resistivity of carbon nanotubes bundles for applications as horizontal interconnects *Appl. Phys. Lett.* **103** 053115
- [52] Song X, Han X, Fu Q, Xu J, Wang N and Yu D P 2009 Electrical transport measurements of the side-contacts and embedded-end-contacts of platinum leads on the same single-walled carbon nanotube *Nanotechnology* **20** 195202
- [53] Chiodarelli N et al 2009 Measuring the electrical resistivity and contact resistance of vertical carbon nanotube bundles for application as interconnects *Nanotechnology* **22** 085302
- [54] Nihei M, Kawabata A, Sato S, Nozue T, Hyakushima T, Norimatsu M, Murakami T, Kondo D, Ohfuti M and Awano Y 2008 Carbon nanotube via interconnects with large current carrying capacity *ICSICT'08: Int. Conf. on Solid-State and Integrated-Circuit Technology* pp 541–3
- [55] Dong L, Youkey S, Bush J, Jiao J, Dubin V M and Chebiam R V 2007 Effects of local Joule heating on the reduction of contact resistance between carbon nanotubes and metal electrodes *J. Appl. Phys.* **101** 024320

- [56] Hertel T, Walkup R E and Avouris P 1998 Deformation of carbon nanotubes by surface van der Waals forces *Phys. Rev. B* **58** 13870
- [57] Knupfer M 2001 Electronic properties of carbon nanostructures *Surf. Sci. Rep.* **42** 1–74
- [58] Zhao J, Buldum A, Han J and Lu J P 2002 Gas molecule adsorption in carbon nanotubes and nanotube bundles *Nanotechnology* **13** 195–200
- [59] Sumanaskera G U, Adu C K W, Fang S and Eklund P C 2000 Effects of gas adsorption and collisions on electrical transport in single-walled carbon nanotubes *Phys. Rev. Lett.* **85** 1096–9
- [60] Leenaerts O, Partoens B and Peeters F M 2008 Adsorption of H₂O, NH₃, CO, NO₂ and NO on graphene: a first-principles study *Phys. Rev. B* **77** 125416
- [61] Pati R, Zhang Y, Nayak S K and Ajayan P M 2002 Effect of H₂O adsorption on electron transport in a carbon nanotube *Appl. Phys. Lett.* **81** 2638–40
- [62] Blackburn J L, Barnes T M, Beard M C, Kim Y H, Tenent R C, McDonald T J, To B, Coutts T J and Heben M J 2008 Transparent conductive single-walled carbon nanotube networks with precisely tunable ratios of semiconducting and metallic nanotubes *ACS Nano* **2** 1266–74
- [63] Zahab A, Spina L, Poncharal P and Marliere C 2000 Water-vapor effect on the electrical conductivity of a single-walled carbon nanotube mat *Phys. Rev. B* **62** 10000–3
- [64] Ifuku R, Nagashio K, Nishimura T and Toriumi A 2013 The density of states of graphene underneath a metal electrode and its correlation with contact resistivity *Appl. Phys. Lett.* **103** 033514
- [65] Collins PG, Bradley K, Ishigami M and Zettl A 2000 Extreme oxygen sensitivity of electronic properties of carbon nanotubes *Science* **287** 1801–4
- [66] Kanbara T, Takenobu T, Takahashi T, Iwasa Y, Tsukagoshi K, Aoyagi Y and Kataura H 2006 Contact resistance modulation in carbon nanotube devices investigated by four-probe experiments *Appl. Phys. Lett.* **88** 053118
- [67] Lee J O, Park C, Kim J J, Kim J, Park J W and Yoo K H 2000 Formation of low-resistance ohmic contacts between carbon nanotube and metal electrodes by a rapid thermal annealing method *J. Phys. D: Appl. Phys.* **33** 1953–6
- [68] Nemeč N, Tománek D and Cuniberti G 2006 Contact dependence of carrier injection in carbon nanotubes: an *ab initio* study *Phys. Rev. Lett.* **96** 076802
- [69] Lan C, Srisungsitthisunti P, Amama P B, Fisher T S, Xu X and Reifenberger R G 2008 Measurement of metal/carbon nanotube contact resistance by adjusting contact length using laser ablation *Nanotechnology* **19** 125703
- [70] Zhang L, Austin D, Merkulov V I, Meleshko A V, Klein K L, Guillorn M A, Lowndes D H and Simpson M L 2004 Four-probe charge transport measurements on individual vertically aligned carbon nanofibers *Appl. Phys. Lett.* **84** 3972–4
- [71] Botman A, Mulders J J L and Hagen C W 2009 Creating pure nanostructures from electron-beam-induced deposition using purification techniques: a technology perspective *Nanotechnology* **20** 372001
- [72] Chai Y, Hazeghi A, Takei K, Chen H Y, Chan P C, Javey A and Wong H-S P 2012 Low-resistance electrical contact to carbon nanotubes with graphitic interfacial layer *IEEE Trans. Electron Devices* **59** 12–19
- [73] Kane A A, Sheps T, Branigan E T, Apkarian V A, Cheng M H, Hemminger J C, Hunt S R and Collins P G 2009 Graphitic electrical contacts to metallic single-walled carbon nanotubes using Pt electrodes *Nano Lett.* **9** 3586–91
- [74] Christy R W 1960 Formation of thin polymer films by electron bombardment *J. Appl. Phys.* **31** 1680–3
- [75] Choi Y R, Rack P D, Frost B and Joy D C 2007 Effect of electron beam-induced deposition and etching under bias *Scanning* **29** 171–6
- [76] Rack P D, Fowlkes J D and Randolph S J 2007 *In situ* probing of the growth and morphology in electron-beam-induced deposited nanostructures *Nanotechnology* **18** 465602
- [77] Randolph S J, Fowlkes J D and Rack P D 2006 Focused, nanoscale electron-beam-induced deposition and etching *Crit. Rev. Solid State Mater. Sci.* **31** 55–89
- [78] Brintlinger T, Fuhrer M S, Melngailis J, Utke I, Bret T, Perentes A, Hoffmann P, Abourida P and Doppelt P 2005 Electrodes for carbon nanotube devices by focused electron beam induced deposition of gold *J. Vac. Sci. Technol. B* **23** 3174–7
- [79] Mølhave K, Madsen D N, Dohn S and Bøggild P 2004 Constructing, connecting and soldering nanostructures by environmental electron beam deposition *Nanotechnology* **15** 1047–53
- [80] Utke I, Hoffmann P and Melngailis J 2008 Gas-assisted focused electron beam and ion beam processing and fabrication *J. Vac. Sci. Technol. B* **26** 1197–276
- [81] Koops H W P, Schossler C, Kaya A and Weber M 1996 Conductive dots, wires, and supertips for field electron emitters produced by electron-beam induced deposition on samples having increased temperature *J. Vac. Sci. Technol. B* **14** 4105–9
- [82] Lau Y M, Chee P C, Thong J T L and Ng V 2002 Properties and applications of cobalt-based material produced by electron-beam-induced deposition *J. Vac. Sci. Technol. A* **20** 1295–302
- [83] Wei B Q, Vajtai R and Ajayan P M 2001 Reliability and current carrying capacity of carbon nanotubes *Appl. Phys. Lett.* **79** 1172–4
- [84] An L and Friedrich C R 2012 Measurement of contact resistance of multiwall carbon nanotubes by electrical contact using a focused ion beam *Nucl. Instrum. Methods Phys. Res. B* **272** 169–72
- [85] Madriz F, Yamada T, Sun X, Nickel J G and Yang C Y 2010 Frequency-independent RC circuit model for one-dimensional carbon nanostructures *IEEE Electron Device Lett.* **31** 263–5
- [86] Vyas A A, Madriz F, Kanzaki N, Wilhite P, Sun X, Yamada T and Yang C Y 2014 Carbon nanofiber interconnect RF characteristics improvement with deposited tungsten contacts *J. Nanosci. Nanotechnol.* **14** 2683–6
- [87] Komuro M, Hiroshima H and Takechi A 1998 Miniature tunnel junction by electron-beam-induced deposition *Nanotechnology* **9** 104–7
- [88] Ominami Y, Ngo Q, Suzuki M, Austin A J, Yang C Y, Cassell A M and Li J 2006 Interface characteristics of vertically aligned carbon nanofibers for interconnect applications *Appl. Phys. Lett.* **89** 263114
- [89] Martel R, Derycke V, Lavoie C, Appenzeller J, Chan K K, Tersoff J and Avouris P 2001 Ambipolar electrical transport in semiconducting single-wall carbon nanotubes *Phys. Rev. Lett.* **87** 256805
- [90] Wang M S, Golberg D and Bando Y 2010 Superstrong low-resistant carbon nanotube–carbide-metal nanocontacts *Adv. Mater.* **22** 5350–5
- [91] Matsuda Y, Deng W Q and Goddard W A 2010 Contact resistance for ‘end-contacted’ metal–graphene and metal–nanotube interfaces from quantum mechanics *J. Phys. Chem. C* **114** 17845–50
- [92] Wang L et al 2013 One-dimensional electrical contact to a two-dimensional material *Science* **342** 614–7
- [93] Ngo Q, Yamada T, Suzuki M, Ominami Y, Cassell A M, Li J, Meyyappan M and Yang C Y 2007 Structural and electrical characterization of carbon nanofibers for interconnect via applications *IEEE Trans. Nanotechnol.* **6** 688–95

- [94] Meyyappan M, Delzeit L, Cassell A and Hash D 2003 Carbon nanotube growth by PECVD: a review *Plasma Sources Sci. Technol.* **12** 205–16
- [95] Cruden B A, Cassell A M, Ye Q and Meyyappan M 2003 Reactor design considerations in the hot filament/direct current plasma synthesis of carbon nanofibers *J. Appl. Phys.* **94** 4070–8
- [96] Zhang Y, Franklin N W, Chen R J and Dai H 2000 Metal coating on suspended carbon nanotubes and its implication to metal–tube interaction *Chem. Phys. Lett.* **331** 35–41
- [97] Lim S C, Choi H K, Jeong H J, Song Y I, Kim G Y, Jung K T and Lee Y H 2006 A strategy for forming robust adhesion with the substrate in a carbon-nanotube field-emission array *Carbon* **44** 2809–15
- [98] Liebau M, Unger E, Duesberg G S, Graham A P, Seidel R, Kreupl F and Hoenlein W 2003 Contact improvement of carbon nanotubes via electroless nickel deposition *Appl. Phys. A* **77** 731–4
- [99] Bayer B C *et al* 2011 *In-situ* study of growth of carbon nanotube forests on conductive CoSi₂ support *J. Appl. Phys.* **109** 114314
- [100] Fayolle M *et al* 2011 Innovative scheme for selective carbon nanotubes integration in via structures *Microelectron. Eng.* **88** 833–6
- [101] Lee S, Lim J S and Baik S J 2011 Integration of carbon nanotube interconnects for full compatibility with semiconductor technologies *J. Electrothermal Soc.* **158** K193–6
- [102] Chiodarelli N, van der Veen M H, Vereecke B, Cott D J, Groeseneken G, Vereecken P M, Huyghebaert Z and Tokei Z 2011 Carbon nanotube interconnects: electrical characterization of 150 nm CNT contacts with Cu damascene top contact *IITC/MAM'11: IEEE Int. Interconnect Technology Conf. and 2011 Materials for Advanced Metallization* pp 1–3
- [103] Subramaniam C, Yamada T, Kobashi K, Sekiguchi A, Futaba D N, Yumura M and Hata K 2013 One hundred fold increase in current carrying capacity in a carbon nanotube-copper composite *Nature Commun.* **4** 2202
- [104] Santini C A, Volodin A, Van Haesendonck C, De Gendt S, Groeseneken G and Vereecken P M 2011 Carbon nanotube–carbon nanotube contacts as an alternative towards low resistance horizontal interconnects *Carbon* **49** 4004–12
- [105] Kong J, Zhou C, Morpurgo A, Soh H T, Quate C F, Marcus C and Dai H 1999 Synthesis, integration, and electrical properties of individual single-walled carbon nanotubes *Appl. Phys. A* **69** 305–8